Steidl, M., Koppka, C., Winterfeld, L., Peh, K., Galiana, B., Supplie, O., Kleinschmidt, P., Runge, E., & Hannappel, T. (2017). Impact of Rotational Twin Boundaries and Lattice Mismatch on III–V Nanowire Growth. *In ACS Nano, 11*(9), 8679–8689

DOI: 10.1021/acsnano.7b01228

Impact of rotational twin boundaries and lattice mismatch on III-V nanowire growth

Journal:	*ACS Nano*
Manuscript ID	nn-2017-012285.R1
Manuscript Type:	Article
Date Submitted by the Author:	n/a

Complete List of Authors:	Steidl, Matthias; Technische Universitat Ilmenau, Department of Photovoltaics, Institute of Physics Koppka, Christian; Technische Universitat Ilmenau, Department of Photovoltaics, Institute of Physics Winterfeld, Lars; Technische Universitat Ilmenau, Theoretical Physics I, Institute of Physics Peh, Katharina; Technische Universitat Ilmenau, Department of Photovoltaics, Institute of Physics Galiana, Beatriz; Universidad Carlos III de Madrid, Physics Department Supplie, Oliver; Technische Universitat Ilmenau, Department of Photovoltaics, Institute of Physics Kleinschmidt, Peter; Technische Universitat Ilmenau, Department of Photovoltaics, Institute of Physics Runge, Erich; Technische Universitat Ilmenau, Theoretical Physics I, Institute of Physics Hannappel, Thomas; Technische Universitat Ilmenau, Department of Photovoltaics, Institute of Physics

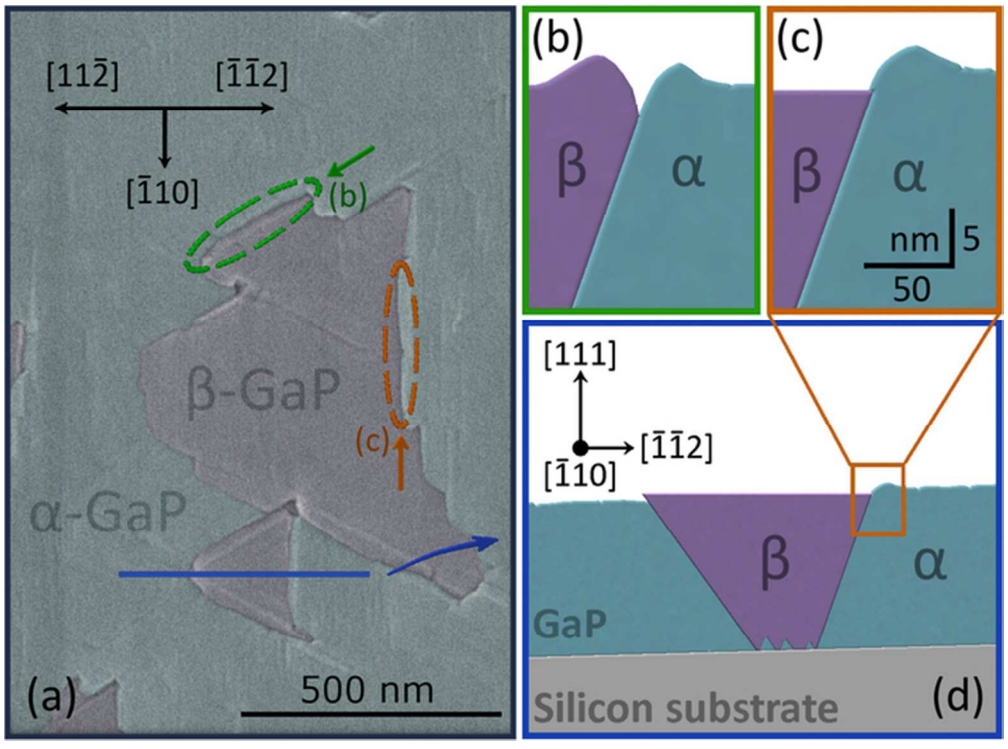

Figure 1. (a) SEM micrograph of several rotational twin domains. The twin boundaries are preferentially aligned along ⟨110⟩ and exhibit a distinct morphology, which is illustrated in (b) and (c) for two different crystallographic directions. Note that the concrete shape in (b) also depends on the exact position on the RTB, while it is more or less independent for (c). (d) displays a schematic side view of a twin domain β within the α-matrix.

60x44mm (300 x 300 DPI)

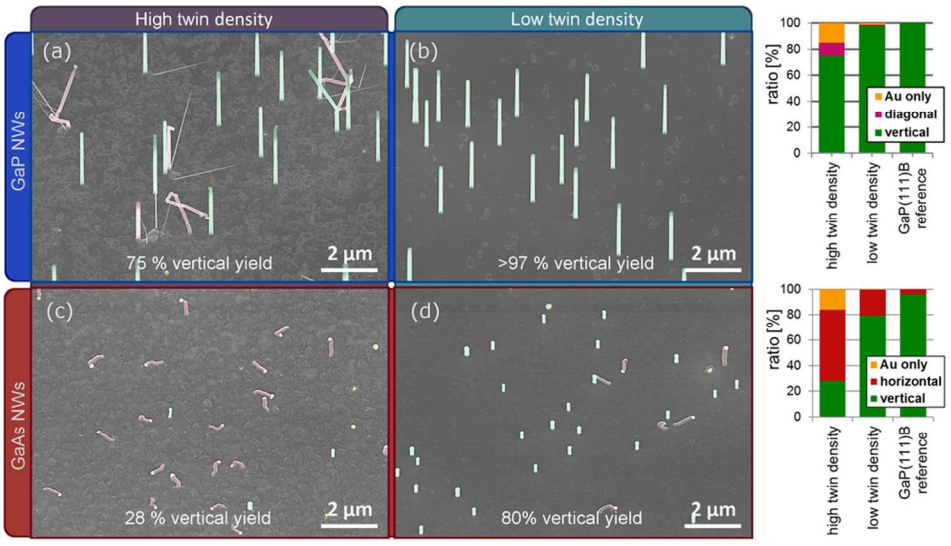

Figure 2. Representative SEM overview scans (30° tilt view) of NWs grown on GaP/Si(111) substrates with different rotational twin density. (a) and (b) display GaP NWs on GaP/Si with high and low twin density, respectively. (c) and (d) show the growth results for GaAs NWs. The side panels contain statistics over the different types of NWs on different substrates including a GaP(111)B wafer piece as reference. Note that the GaAs NW growth time was set intentionally short, resulting in short NWs for an easier characterization. This, in turn, leads to different visibilities of the twin boundaries for the GaP and GaAs NW samples.

90x48mm (300 x 300 DPI)

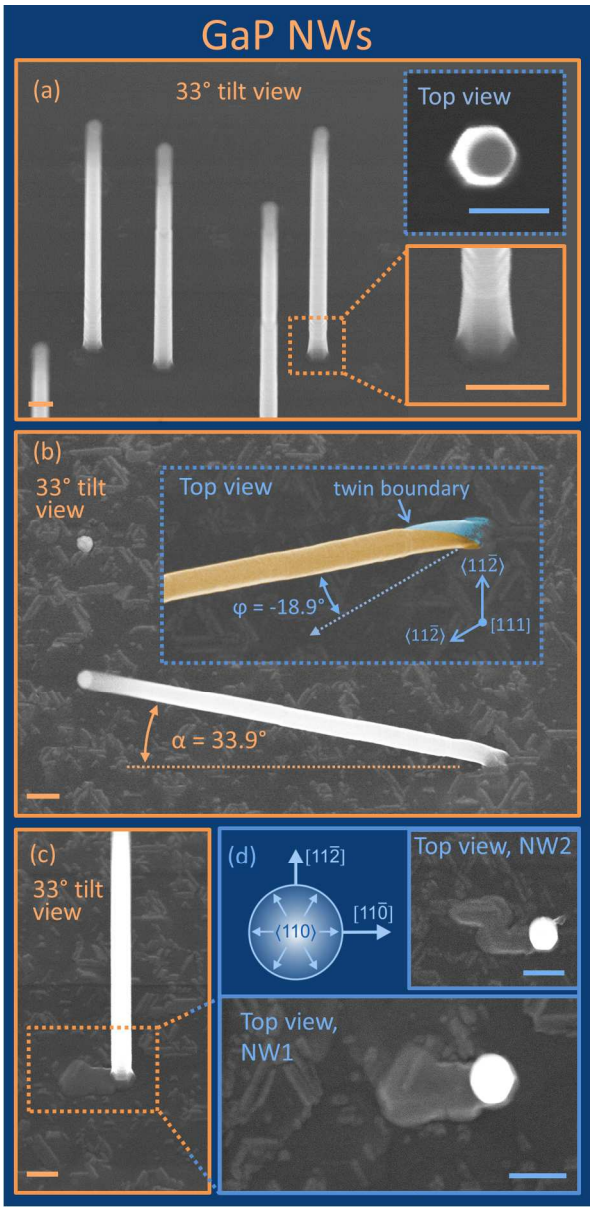

Figure 3. Different types of GaP NWs on GaP/Si substrates. (a) A group of typical vertical NWs exhibiting a hexagonal cross section (upper inset) and grooves at the facets reflecting stacking faults within the NW (lower inset). (b) Diagonal NW emerging at a rotational twin boundary (RTB). The angle α is the angle with the substrate (111)-surface and ϕ is the azimuthal angle to the next ⟨11-2⟩ direction according to Ref. 42. (c) Initially horizontal NW aligned along an RTB in ⟨110⟩ growing vertically outside the RTB. (d) shows the NW from (c) from the top and another NW initially growing horizontally along an RTB. All scale bars are 200 nm.

167x340mm (300 x 300 DPI)

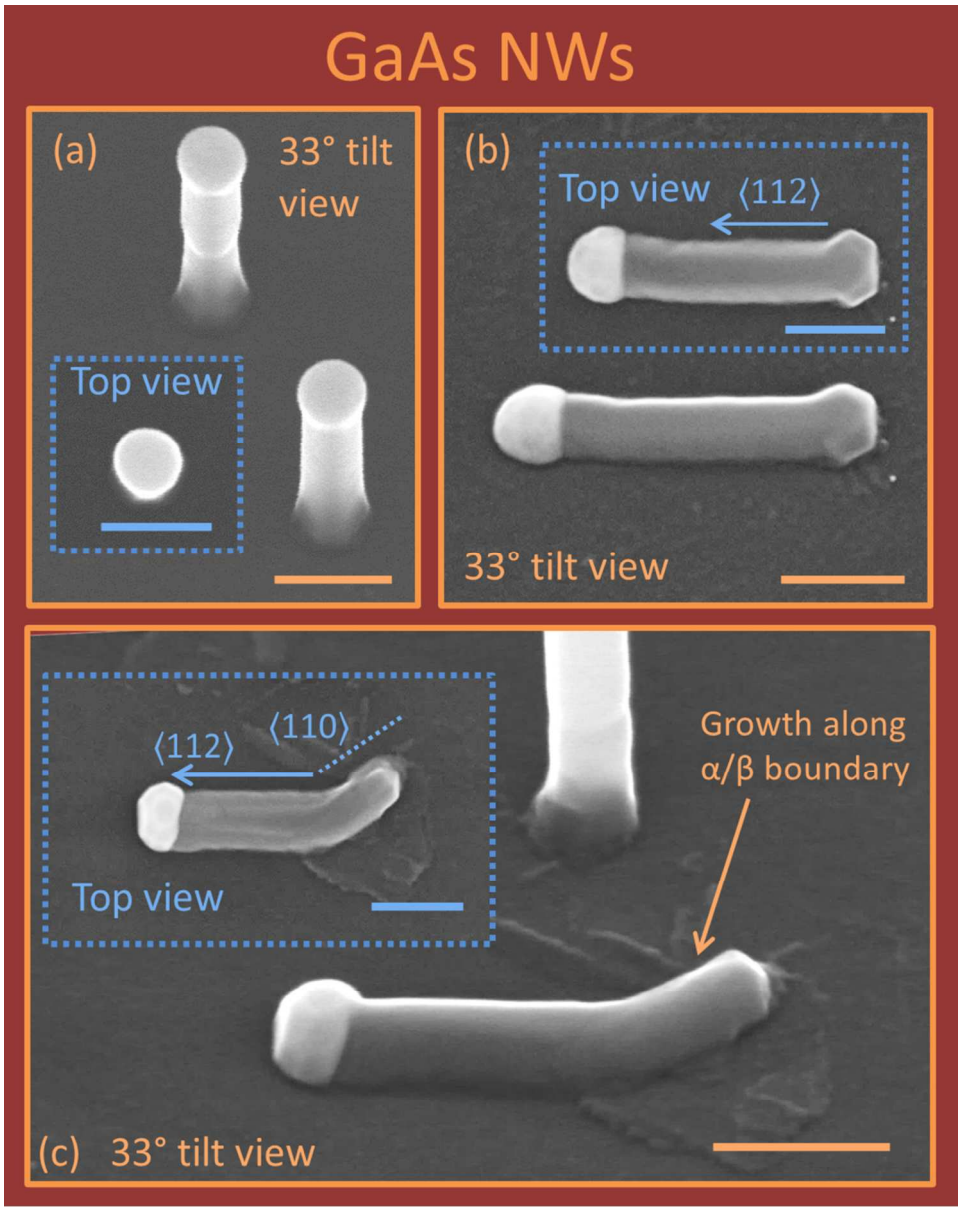

Figure 4. Different types of GaAs NWs on GaP/Si substrates. (a) Two typical vertical NWs. The upper NW's bulge reflects (at least) a stacking fault within the NW. (b) Horizontal NW pointing in ⟨112⟩ without a noticeable substrate defect. (c) Horizontal NW growing at first along a twin boundary in ⟨110⟩ and then in ⟨112⟩ departing from the twin. All scale bars are 200 nm.

103x129mm (300 x 300 DPI)

(1) (2') (2)

Substrate S

GaP(1

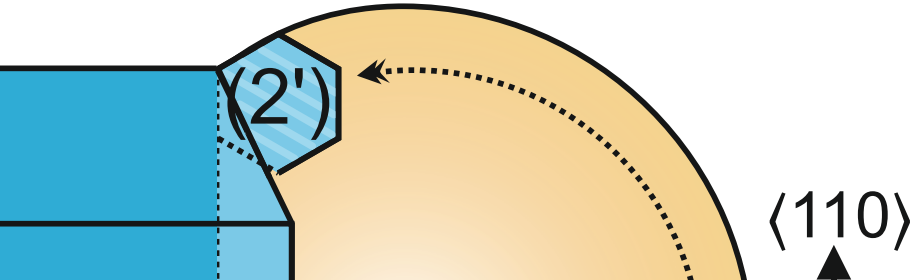

d)

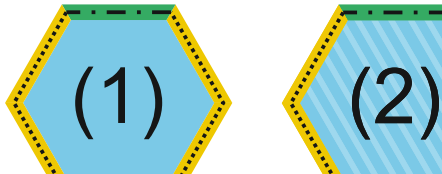

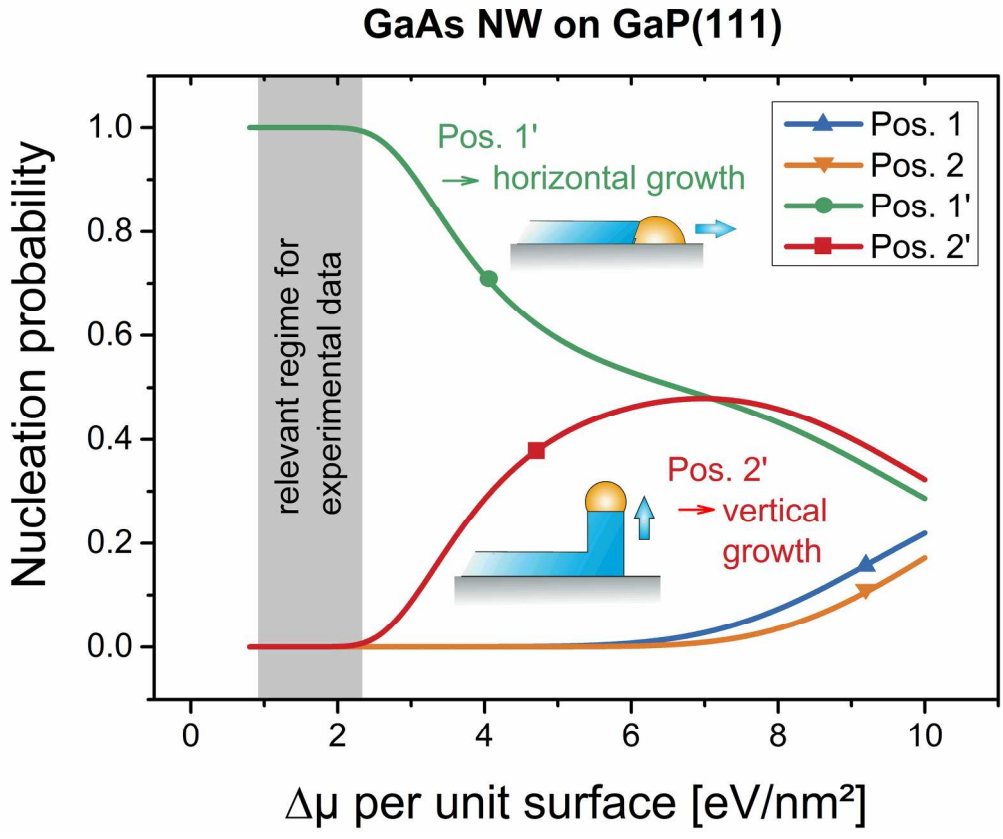

Figure 6. The probability for different nuclei in dependence of the chemical potential difference Δμ calculated for a horizontal GaAs NW on GaP assuming hexagonally shaped nuclei. The range of Δμ relevant for the experiments is highlighted in blue.

194x161mm (300 x 300 DPI)

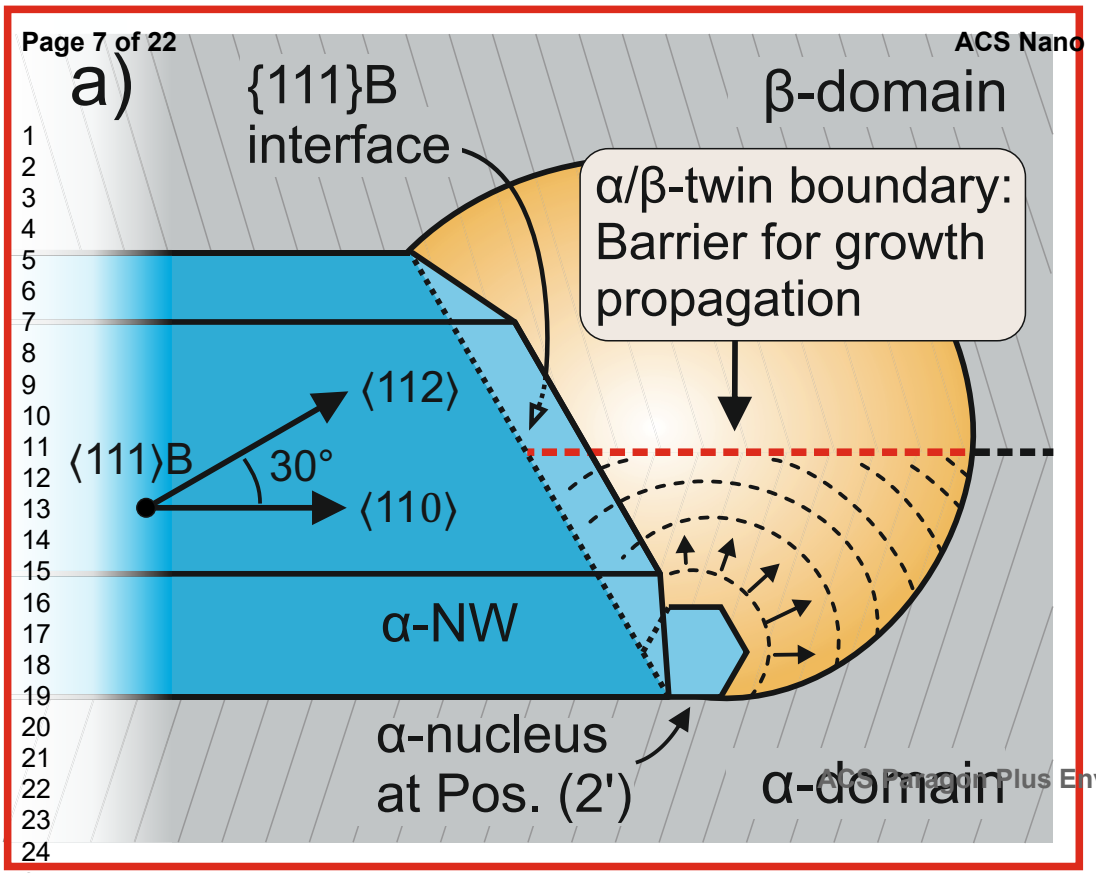

Nucleation at Pos (2'):
→ impeded (vertical) growth

Nucleation at Pos (1'):
→ unhindered horizontal growth

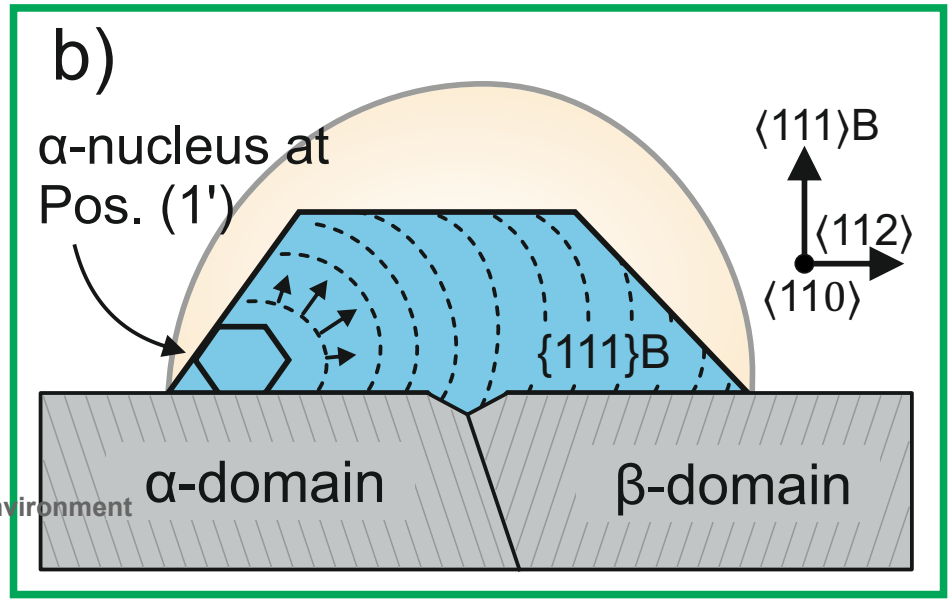

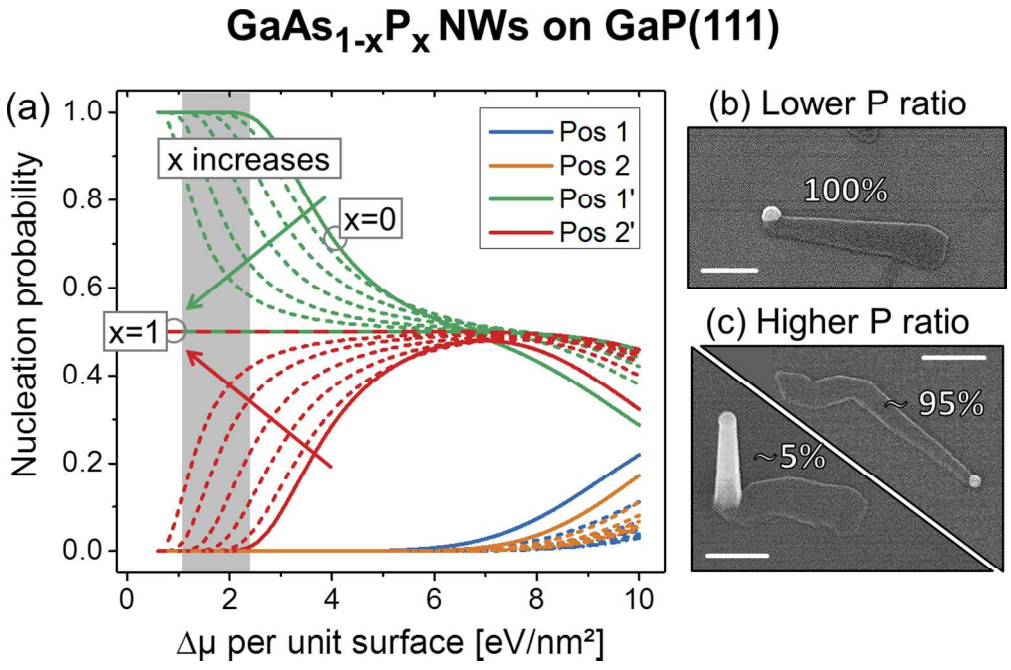

Figure 8. (a) Nucleation probabilities for horizontal GaAs1-xPx NWs grown on GaP(111)B with x ranging from 0 to 1 (x∈ {0, 0.05, 0.1, 0.2, 0.35, 0.6, 1}), i.e. pure GaAs and GaP, respectively. Geometrical parameters are chosen in analogy to Figure 6 and interfacial energies are interpolated linearly between both extremes (cf. section S9). (b) and (c) show horizontal GaAsP NWs on GaP(111)B with two different compositions. While for the lower P ratio all NWs remain horizontal, around 5% of the NWs become vertical for the higher P ratio. The scale bars are 200 nm. For SEM overview scans the reader is referred to Figure S13 in the Supporting Information.

113x73mm (300 x 300 DPI)

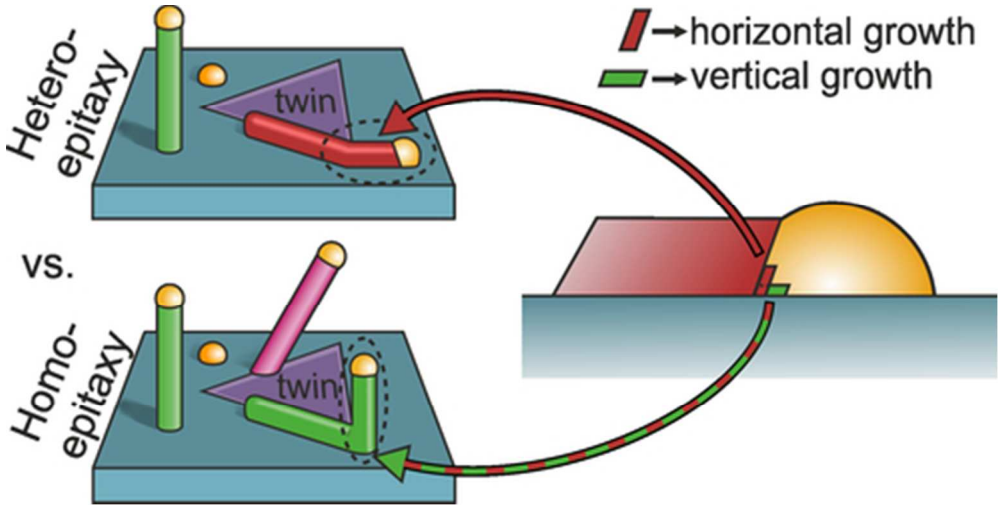

TOC figure

41x21mm (300 x 300 DPI)

Impact of rotational twin boundaries and lattice mismatch on III-V nanowire growth

Matthias Steidl[1]*, Christian Koppka[1‡], Lars Winterfeld[2‡], Katharina Peh[1], Beatriz Galiana[3], Oliver Supplie[1], Peter Kleinschmidt[1], Erich Runge[2], Thomas Hannappel[1]*

[1] Department of Photovoltaics, Institute of Physics and Institute of Micro- and Nanotechnologies, TU Ilmenau, 98693 Ilmenau, Germany

[2] Department of Theoretical Physics I, Institute of Physics and Institute of Micro- and Nanotechnologies, TU Ilmenau, 98693 Ilmenau, Germany

[3] Physics Department, Universidad Carlos III de Madrid, 28911 Madrid, Spain

Supporting Information Placeholder

ABSTRACT: Pseudomorphic planar III-V transition layers greatly facilitate the epitaxial integration of vapor-liquid-solid grown III-V nanowires (NW) on Si(111) substrates. Heteroepitaxial (111) layer growth, however, is commonly accompanied by the formation of rotational twins. We find that rotational twin boundaries (RTBs), which intersect the surface of GaP/Si(111) hetero-substrates, generally cause horizontal NW growth and may even suppress NW growth entirely. Away from RTBs, the NW growth direction switches from horizontal to vertical in case of homoepitaxial GaP NWs, whereas heteroepitaxial GaAs NWs continue growing horizontally. To understand this rich phenomenology, we develop a model based on classical nucleation theory. Independent of the occurrence of RTBs and specific transition layers, our model can generally explain the prevalent observation of horizontal III-V NW growth in lattice mismatched systems and the high crystal quality of horizontal nanowires.

The epitaxial integration of III-V nanowires (NWs) with silicon has attracted considerable interest as one of the most promising routes of combining the tunable, high-performance properties of III-V materials with the well-established Si technology.[1–4] The Au-mediated vapor-liquid-solid (VLS) growth discovered by Wagner *et al.*[5] is a widely used, powerful technique for the fabrication of III-V NWs.[6–8] However, direct growth of III-V NWs on Si encounters several difficulties. The strong chemical interaction between Au and the Si[9,10] can cause unintentional doping of the NWs with Si[1] as well as deep level defects induced by diffusion of Au into Si.[11,12] Furthermore, obtaining abrupt interfaces towards Si[10] and a reproducible, adequate substrate pretreatment[3] are challenging tasks. In addition, the condition of the growth reactor plays a crucial role.[13,14] To overcome these difficulties, a III-V transition layer can be grown prior to NW growth (often referred to as (III-V-on-Si) virtual substrates or quasi-substrates). This approach was implemented successfully for various III-V NWs such as GaAs,[15,16] InP,[4] InAs[17] and GaN[18,19] NWs. In these studies, (111) oriented substrates were used, as NWs preferably grow in [111] direction, and well-defined NWs oriented vertical to the substrate surface are advantageous for most device architectures.

Heteroepitaxial layer growth on (111) oriented substrates, however, is usually accompanied by the occurrence of rotational twins, which introduce a considerable density of grain boundaries. Despite the expected detrimental effects of these defects on optoelectronical properties, this issue has received only little attention so far, both in studies focusing on NW growth and those rather addressing the layer preparation. In many studies, the occurrence of rotational twins is not mentioned and discussed at all, although they are obviously present and clearly visible in electron microscopical images.[4,15] In other cases, if recognized[16] or studied in detail,[20,21] either no NW growth is carried out or their impact on NW growth is not further discussed.[16] In a recent study,[22] we demonstrated the importance of the GaP/Si(111) nucleation route on the formation of rotational twins and showed that we are able to suppress the density of twins to around 5 vol%.

Here, we present a systematic investigation of the impact of rotational twin boundaries (RTBs) and lattice mismatch on NW growth and their growth directions. For this purpose, GaP(111) transition layers with B-type polarity[23] and different twin densities are prepared on Si(111) (according to Ref. 22) and either GaP or GaAs NWs are grown subsequently by the Au-mediated VLS mechanism. It is shown, that the growth characteristics of homoepitaxial NWs (*i.e.* GaP) and heteroepitaxial NWs (*i.e.* GaAs) share many similarities, but also differ in some significant aspects. This is important to notice as most of the aforementioned studies that employ transition layers are limited to homoepitaxial NW growth.[4,15–17,22] One

key observation of our study is that both GaP and GaAs NWs grow horizontally along a twin boundary, when growth is initiated at this defect. However, as soon as the NW leaves the twin boundary, GaP NWs change their growth direction towards the vertical [111] direction, while GaAs NWs remain horizontal.

In order to explain the different growth behaviors of homo- and heteroepitaxial NWs, we developed a theoretical model based on classical nucleation theory and preferential interface nucleation.[24] This model builds upon previous experimental and theoretical studies advocating classical nucleation theory to explain VLS NW growth itself[25,26] and to describe several related growth phenomena.[25,27–32] These studies however, exclusively deal with freestanding NWs. In our model we adopt the basic ideas to explain and describe horizontal growth along substrate surfaces with and without RTBs. Our calculations reveal that strain alone (induced by lattice mismatch between NW and substrate) can be decisive for the final growth direction. Beyond the issue of rotational twins, our model can be applied to explain in more depth the prevalent observation of horizontally grown NWs (often referred to as planar, or lateral or in-plane NWs) in other lattice-mismatched systems such as InAs(Sb) NWs on GaAs(111)B[33] or Si,[34] GaAs NWs on Si(111),[35] InAs NWs on GaAs(100)[36,37], various III-V NWs on graphite or graphene[38,39] and II-VI NWs on sapphire.[40–43]

Results and discussion

Rotational twin domains

Epitaxy of semiconductors on (111) oriented substrates involves the problem of the formation of rotational twins (shown in Figure 1 with violet highlighting for GaP on Si(111) used in this study). The growth of twinned GaP (referred to as β-GaP in the α-GaP matrix) is caused by an alternative orientation of the cubic lattice at the interface to the substrate. This so-called cis-coordination can be formally described by a rotation of the GaP lattice around the [111] axis normal to the surface of the silicon substrate by 60°. These twinned GaP parts are typically grouped together into large domains (see Figure 1a and d). The resulting lateral RTBs can penetrate through the entire GaP epilayer and reach the surface (*cf.* Figure 2 of Ref. 44). Here, they form trenches that are a few nm deep and preferably oriented along ⟨110⟩ directions (for sake of simplicity also referred to as RTBs). For 100 nm thick GaP epilayers, rotational twin domains (RTDs) can be observed with diameters typically ranging from a few 100 nm up to several µm. HR-XRD results show that the β-GaP density and domain size is significantly affected by the GaP nucleation and therefore varies strongly with the nucleation

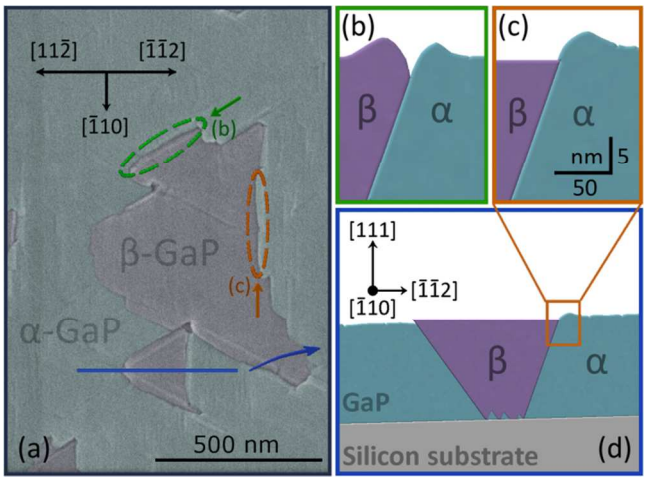

Figure 1. (a) SEM micrograph of several rotational twin domains. The twin boundaries are preferentially aligned along ⟨110⟩ and exhibit a distinct morphology, which was determined by atomic force microscopy and is illustrated in (b) and (c) for two different crystallographic directions. Note that the specific shape in (b) also depends on the exact position on the RTB, while it is more or less independent for (c). (d) displays a schematic side view of a twin domain β within the α-matrix.

conditions and substrate misorientation.[22] RTBs have a major influence on the resulting GaP surface morphology. A reduction of the β-GaP density causes a significant reduction of the RTB density, which considerably reduces the surface roughness. Besides this dominant effect of the domain boundaries, the roughness within individual β-domains is smaller than that of α-domains (rms roughness of ~0.56 nm and ~0.87 nm, respectively). The latter show a textured morphology, which is presumably caused by the step structure of the vicinal substrate (in this work Si(111) substrates with 3° miscut in [11-2] direction were used). Due to the miscut of the substrates, the β-domain surface seems to be 'tilted' with respect to the α-domain surface. This results in two different types of trenches along the domain boundaries as illustrated in Figure 1b and c. The GaP layers were shown to consist completely of B-type polarity material by low-energy electron diffraction (LEED) measurement.[23] We observed only (1x1) surface reconstruction even in the case of highly twinned GaP layers, whereas {111}A-type material would result in half-order spots, *i.e.* (2x2) reconstruction. Hence, we can exclude the presence of {111}A-type polar surfaces (inversion domains as considered in Ref. 45) and potential influence on NW growth.

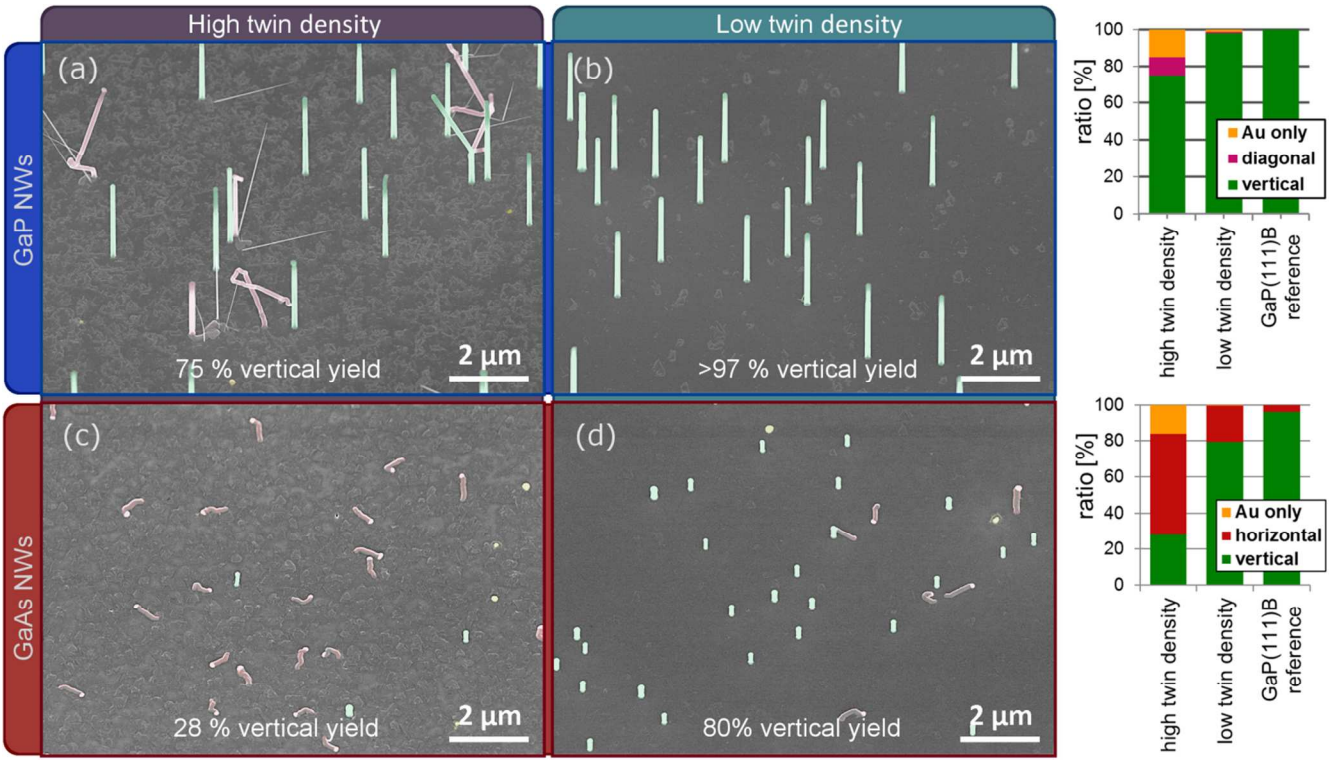

Figure 2. Representative SEM overview scans (30° tilt view) of NWs grown on GaP/Si(111) substrates with different rotational twin density. (a) and (b) display GaP NWs on GaP/Si with high and low twin density, respectively. (c) and (d) show the growth results for GaAs NWs. The side panels contain statistics over the different types of NWs on different substrates including a GaP(111)B wafer piece as reference. Note that the GaAs NW growth time was set intentionally short, resulting in short NWs for an easier characterization. This, in turn, leads to different visibilities of the twin boundaries for the GaP and GaAs NW samples.

Impact of rotational twin boundaries on nanowire growth

The strong impact of RTBs on the NW growth becomes immediately apparent in overview SEM scans such as shown in Figure 2. Parts a and b compare GaP NW growth on GaP/Si(111) substrates with two different twin densities. The side panel indicates the ratio of different NW types as a function of the substrate type. On GaP films with high twin density (Figure 2a), only 75% of the NWs are vertical to the substrate and a significant amount of NWs exhibits undesired growth directions and morphologies such as NWs inclined to the substrate (referred to as 'diagonal NWs'). These NWs grow diagonally to the substrate surface directly from the start and tend to undergo multiple changes of the growth direction afterwards. Furthermore, Au particles without NW growth are observed (referred to as 'Au only') and a multitude of thin parasitical NWs – mostly non-vertical – is present. Note that we call NWs, which are initially vertical and kink later on, still 'vertical'. All these undesired phenomena can be drastically reduced by employing GaP/Si(111) substrates with a low twin density instead, so that the yield of vertical NWs exceeds 97%. Before we discuss all the different types of GaP NWs in detail, we address the growth of GaAs NWs.

For GaAs NWs the same trend is observed. Here, growth of NWs on GaP(111)/Si substrates with a high twin density yields only 28% of vertical NWs (Figure 2c), while a reduction of the twin density can increase the yield significantly to up to 80% (Figure 2d). In contrast to GaP NWs, neither diagonal nor kinked NWs are observed for GaAs NWs. Instead, NWs growing horizontally along the substrate represent the main defect type (besides Au-particles without NWs). As will be discussed later, these NWs frequently change their growth direction in plane, but never out of plane. In other words, they always remain horizontal.

Comparing GaP and GaAs NWs, *i.e.* Figure 2a with c and Figure 2b with d, it is clearly visible that the growth of vertical heteroepitaxial NWs (*i.e.* GaAs) is much more challenging. On the one hand, this is due to the inherently impeded growth of GaAs NWs on GaP (see statistics in Figure 2 for the reference sample with GaP(111)B wafer piece); on the other hand, the GaAs NW growth is more sensitive to defects at the substrate surface, in particular to RTBs (*cf.* section S3 of the Supporting Information). The statistical data shown in the side panels demonstrate impressively that the detrimental effect of RTBs on the yield of vertical NWs is more pronounced for heteroepitaxial NWs, where the vertical yield is more than doubled when growth is carried out on the substrate with low twin density (Figure 2d vs. c).

Growth directions of GaP nanowires

Figure 3 shows different types of GaP NWs which will be discussed in the following: (a) vertical NWs, (b) diagonal NWs, and (c) NWs changing their growth direction from horizontal to vertical. Growth in the vertical [111]B direction represents the regular and desired growth direction,[46] and is observed if NW nucleation proceeds without detrimental

influences caused by the substrate surface properties (such as RTBs or other defects). The vertical GaP NWs in Figure 3a exhibit a hexagonal cross section with {112} side facets. These side facets are characterized by more or less equidistant bulges reflecting stacking faults within the NW,[30,47] which are typical for III-V NWs grown in [111]B direction.[27,47,48] Note that some of the initially vertical NWs are kinked in the upper part of the NW (see Figure 2a). We attribute this behavior to process-related growth instabilities and exclude an impact of RTBs, since this behavior is observed for growth on the GaP(111)B reference substrate to the same extent (Figure S1a in the Supporting Information).

Diagonal NWs, in contrast, such as the one shown in Figure 3b, are directly related to RTBs as they are only observed when emerging at RTBs. Since these NWs also have a hexagonal cross section and overall the same morphology as the vertical NWs, we conclude that the diagonal NWs grow in a ⟨111⟩B direction. This conclusion is further supported by growth of GaP NWs on a GaP(111)A substrate. Here, the small fraction of vertical NWs exhibits an overall different morphology characterized by truncated triangular cross section segments that are rotated by 60° every 300 nm (see inset of Figure S1b in the Supporting Information). The vast majority of the diagonal NWs can be explained with (multiple) twinning at {111} facets within the NW bottom according to Uccelli *et al.*[49] Following their definition, α describes the angle between the NW and the substrate (111) plane and φ the azimuthal angle towards the next ⟨11-2⟩ direction. In the case of the NW shown in Figure 3b, α is 33.9° and φ equals -18.9°, which is in very good agreement with the theoretical predictions from Uccelli *et al.* for 1st order twinning (2nd order seed with B-type polarity, α = 33.8°, φ = ±19.1°). Moreover, the twinning planes, which are within the NW and in contact with the substrate, can be clearly seen. For better visibility the two NW segments are color-coded in the top view inset of Figure 3b. Figure S3 in the Supporting Information shows pairs of angle values (α and φ) for another 75 diagonal NWs. With a tolerance of ±5° for both α and φ, 65% of the NWs can be assigned to 2nd and 3rd order B-type (polarity) nuclei (1st order and 2nd order twinning, respectively). Only a small percentage of 9% undergoes more twinning processes in the initial stage. Moreover, only very few NWs can be assigned to A-type NWs, which is in agreement with the finding that the inspected diagonal NWs exhibit a hexagonal cross section and are consequently B-type. A likely explanation for the formation of these diagonal NWs is the following. Any Au droplet at an RTB initially wets both the α- and the β-domain. When growth begins, nucleation events and growth occur on both domains leading to a twin boundary within the NW. The higher the contact area between the Au droplet and a NW part, the greater the nucleation probability at the respective interface. Therefore, one crystallographic orientation is favored over the other one and, thus, determines the final crystal orientation of the NW.

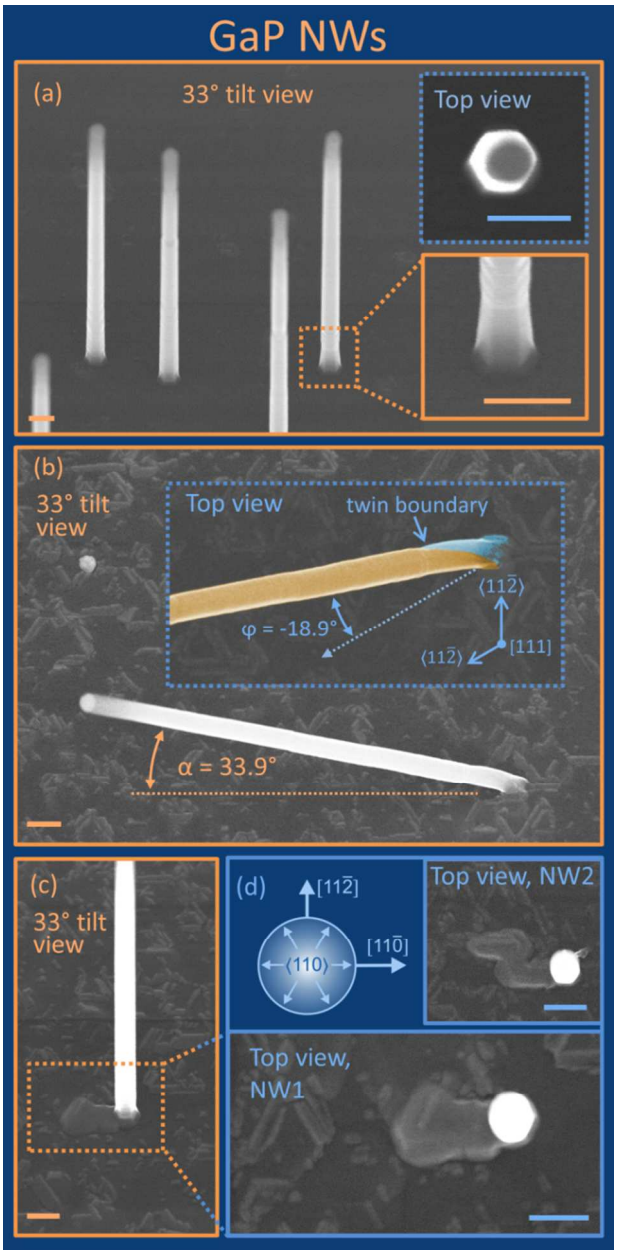

Figure 3. Different types of GaP NWs on GaP/Si substrates. (a) A group of typical vertical NWs exhibiting a hexagonal cross section (upper inset) and grooves at the facets reflecting stacking faults within the NW (lower inset). (b) Diagonal NW emerging at a rotational twin boundary (RTB). The angle α is the angle with the substrate (111)-surface and ϕ is the azimuthal angle to the next ⟨11-2⟩ direction according to Ref. 49. (c) Initially horizontal NW aligned along an RTB in ⟨110⟩ growing vertically outside the RTB. (d) shows the NW from (c) from the top and another NW initially growing horizontally along an RTB. All scale bars are 200 nm.

We continue with a growth phenomenon which is particularly relevant for the growth on GaP/Si(111) substrates with a high twin density. Figure 3c and d give examples of GaP NWs growing horizontally in a ⟨110⟩ direction, where the NWs drastically change their growth direction towards the vertical [111]B direction when they leave the vicinity of the twin boundary. This behavior is observed for all initially horizontal GaP NWs. Horizontal (planar) NW growth along ⟨110⟩ has not been reported before. Typically, horizontal NW growth occurs in ⟨112⟩ directions,[33,35,50] which is also observed in this study for horizontal GaAs NWs on GaP(111)B (see Figure 5b and S2 in the Supporting Information). Here, the growth facet is one of the {111} planes and the projection of the corresponding ⟨111⟩ direction on the surface is aligned with the growth direction. This shows that horizontal growth occurs *along* an RTB, although the RTB is covered by the NW and thereby not always directly visible. Three questions arise: 1. Why does horizontal growth occur at all? 2. Why does it not occur in a ⟨112⟩ direction but along the RTB? 3. Why does a NW change its growth direction into the vertical direction, when it departs from an RTB? We first address question 2: We have observed in all our experiments that Au-particles are preferentially trapped at RTBs. Directly after Au-deposition, only ~10% of the particles are located at an RTB. After annealing (at 600°C for 10 min) the proportion rises (reproducibly) to ~40%. This shows on the one hand that the Au-particles are mobile at these conditions and on the other hand that they get trapped at RTBs; the latter can be explained by a reduction of the total interface energies when a Au-particle covers the trench of a RTB. When NW growth occurs, the Au-particle will stay at the RTB and be shifted along the RTB in ⟨110⟩ with material precipitating at the Au/NW interface, which is most likely a {111} plane, too. Consequentially, the growth direction ⟨110⟩ and the projection of the normal vector of the growth front on the surface ⟨112⟩ are separated by an azimuthal angle of 30°, as depicted in Figure 7a below. The answer to the 1st and 3rd question requires a detailed nucleation model and will be discussed in the section 'Nucleation model'.

Growth directions of GaAs nanowires

Figure 4a shows two vertical GaAs NWs along [111] direction, which represents, in analogy to GaP NW growth, the desired, regular growth direction. The vertical NWs possess a hexagonal cross section with {112} side facets. The bulge of the upper NW clearly indicates the presence of stacking faults in this region and represents a frequently observed phenomenon for all the vertical GaAs NWs that have been investigated. As mentioned before, GaAs NWs on GaP(111)B substrates tend to grow horizontally on the substrate. This behavior is associated with two aspects: On the one hand growth of vertical GaAs NWs on GaP is inherently impeded, which also leads to horizontal NWs on reference samples with a GaP(111)B wafer substrate (see statistics in Figure 1 and Figure S2 of the Supporting Information). Here, horizontal NWs are preferentially aligned in ⟨112⟩. The same behavior is observed for GaAs NWs on GaP/Si(111) provided that there is no relevant defect on the substrate surface (see Figure 4b). On the other hand the occurrence of horizontal NWs is directly related to the presence of surface defects such as RTBs. The NW presented in Figure 4c originates at an RTB and initially extends horizontally along the RTB in ⟨110⟩ direction. This means that the RTB guides horizontal growth in the same way as for the GaP NWs presented in Figure 3c. The horizontal GaAs NW, however, remains horizontal after escaping the RTB and alters its growth direction towards ⟨112⟩ – and back to ⟨110⟩ in case of encountering another RTB. For this type of NW, other horizontal NW types and additional information the reader is referred to section S3 in the Supporting Information.

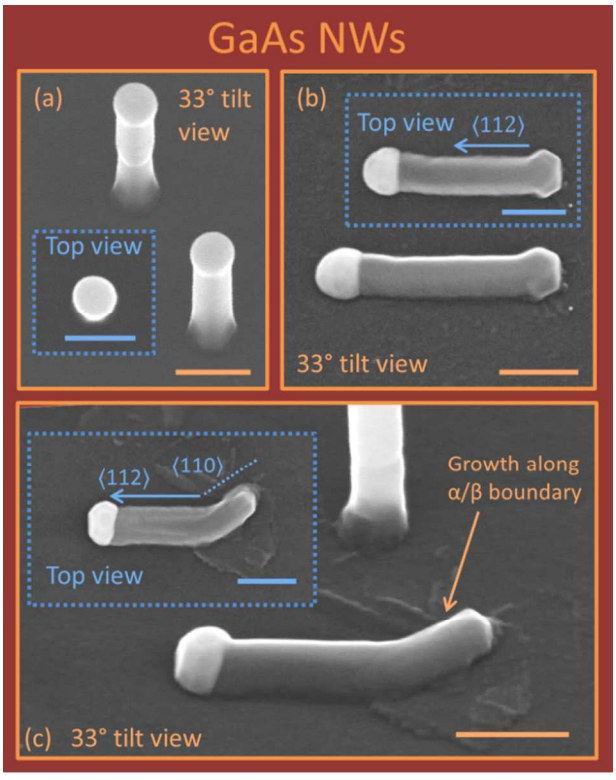

Figure 4. Different types of GaAs NWs on GaP/Si substrates. (a) Two typical vertical NWs. The upper NW's bulge reflects (at least) a stacking fault within the NW. (b) Horizontal NW pointing in ⟨112⟩ without a noticeable substrate defect. (c) Horizontal NW growing at first along a twin boundary in ⟨110⟩ and then in ⟨112⟩ departing from the twin. All scale bars are 200 nm.

Nucleation model

In this section we present a quantitative model, based on classical nucleation theory and preferred interface nucleation.[24] Within this context we will explain why horizontal NWs always remain horizontal in case of heteroepitaxial NW growth while in case of homoepitaxial NW growth, they change their growth direction towards the vertical [111] direction, when no RTB is present.

Classical nucleation theory has very successfully been applied to explain VLS NW growth itself[25,26] and to describe several related growth phenomena such as the simultaneous occurrence of zinc blende and wurtzite[25,27–29] as well as the NW facet formation.[30–32] For the Au-mediated VLS mechanism (and most other metallic catalyst materials) the nucleation of a 2D nucleus is predicted, which forms at the triple phase boundary (TPB), where the vapor, liquid (nanoparticle catalyst) and solid phase (NW) meet.[25,26] Once a stable nucleus has formed, it will quickly extend laterally in all directions until the TPB is reached: Thus, generally a complete NW slice is created before the next nucleation event takes place.

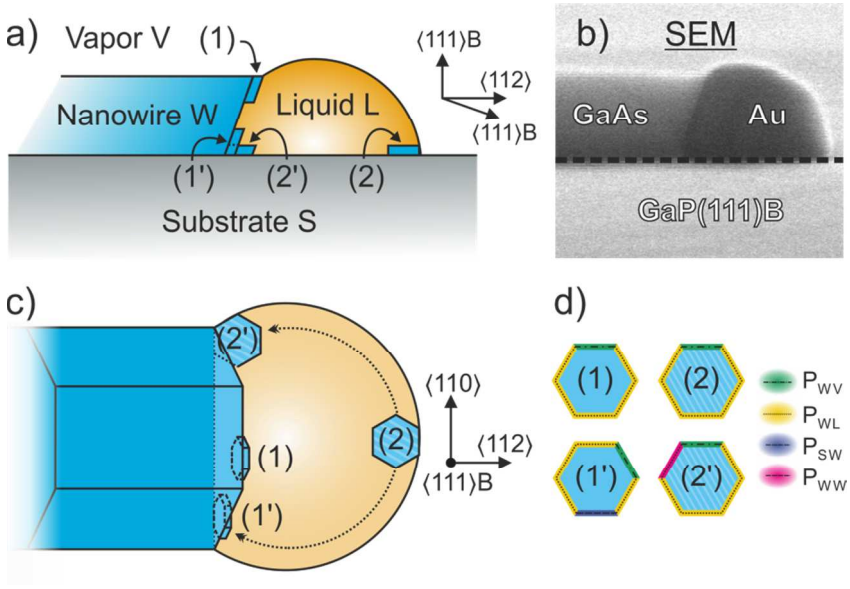

Figure 5. Nucleation model with horizontal NW pointing in ⟨112⟩ – side view both schematically (a) and by SEM (b), and top view (c). The relevant nuclei positions and involved phases are marked. (d) Top view on relevant nuclei and their respective lateral interfaces. The hatching indicates the interface with the underlying substrate.

This mechanism is referred to as 'birth and spread' growth and has also been observed by *in-situ* TEM measurements.[51] The above mentioned studies exclusively deal with freestanding NWs – NWs where the growth front is only in touch with the vapor, the catalyst (in most cases Au) and the NW itself (*i.e.* without contact to the substrate). In our model, we adopt these basic ideas in order to explain and describe horizontal NW growth along a substrate surface.

We start with NW growth outside RTDs. In a birth-and-spread picture, the growth direction of the NWs is determined by the position and orientation of the nuclei. Nucleation is very likely to start at phase boundaries since preexisting interfaces are eliminated.[25] In our case, the relevant positions as marked in Figure 5a are the TPB with positions (1) and (2) as well as the quadruple phase boundaries (QPB) with positions (1') and (2'). Generally, nucleation at positions (1) and (1') will result in an additional layer at the end of the NW (material W, GaAs or GaP) and thereby cause elongated horizontal growth of the wires. On the other hand, nucleation at positions (2) and (2') will result in a layer of material W on top of the substrate S (always GaP) and subsequent vertical NW growth. In the following, L and V denote the liquid or vapor phase, respectively. We have chosen the geometry sketched in Figure 5a to resemble the SEM image in Figure 5b. Due to the stability of the (111) surface for both GaAs and GaP, the W-L interface is almost always (111)-terminated. This explains the angle of approx. 70.5° between substrate and W-L interface. More side views on horizontal NWs exhibiting a (111) growth facet can be found in Figure S8 of the Supporting Information.

In order to quantify the probabilities for nucleation p_i at each position ($i = 1,1',2,2'$), we resort to classical nucleation theory. At growth temperature T, these probabilities are $p_i \propto \exp\left[-\frac{\Delta G_i^*}{k_B T}\right]$, where ΔG_i^* is the change in Gibbs free enthalpy at the critical nucleus radius r_i. Hence, nucleation is preferred if ΔG_i^* is low. Since ΔG_i compares the Gibbs free enthalpy before and after nucleation at constant temperature and pressure, we can write it in the form $\Delta G_i = -N\Delta\mu + \Delta I_i$ with ΔI_i as the additional interface energy introduced by the nucleus and $\Delta\mu > 0$ as the difference in chemical potential of a III-V-pair between liquid and solid phase. The interface energy ΔI_i can be split into one part stemming from the interface area A (parallel to the substrate) and one part from the lateral area P (nucleus circumference × effective height $\tilde{h}$), *i.e.* $\Delta I_i = P\Gamma_i + A\Delta\gamma_i$. Due to the inclination of the nucleus facets, the effective height $\tilde{h} = h/\sin(70.5°)$. The dimension of both Γ_i and γ_i is energy per area.

It is crucial to study ΔI_i in detail for each of the possible configurations. We start with a nucleus at position (1) growing homoepitaxially on W. The nucleus shifts the W-L interface (parallel to W(111)) towards the liquid and creates an additional lateral interface area. We introduce α_1 as the fraction of the lateral area P that is in contact with the vapor phase (highlighted in green in Figure 5d), where the L-V interface is replaced by a W-V one. The rest of P, *i.e.* a fraction $(1-\alpha_1)$, forms a new W-L interface (highlighted in yellow). With the corresponding interface energies γ_{WV} and γ_{WL} (in units of energy per area), we obtain at position (1):

$$\Delta I_1 = P(\alpha_1(\gamma_{WV} - \gamma_{LV}) + (1-\alpha_1)\gamma_{WL}) \qquad (1)$$

Note that for the sake of clarity and concreteness, we depict the nuclei in hexagonal shape in Figure 5 - in this case $\alpha = 1/6$. We keep the formulas in a general form, which allows us to briefly discuss other nuclei shapes in section S8 of the Supporting Information. Position (1') differs from (1) in that a fraction $\beta_{1'}$ (highlighted in blue) is in contact with the substrate rather than with the liquid. Hence, a S-L interface is replaced with a S-W one, while the rest of P, *i.e.* a fraction $(1-\alpha_1-\beta_{1'})$, introduces a new W-L interface:

$$\Delta I_{1'} = P(\alpha_{1'}(\gamma_{WV} - \gamma_{LV}) + \beta_{1'}(\gamma_{SW} - \gamma_{SL}) + (1-\alpha_{1'}-\beta_{1'})\gamma_{WL}) \qquad (2)$$

Position (2) differs from (1) and (1') in so far as the nucleus grows on the substrate material S rather than on W. The S-L

interface of area A is thus replaced with a W-L and an additional S-W interface. Therefore:

$$\Delta I_2 = P(\alpha_2(\gamma_{WV} - \gamma_{LV}) + (1 - \alpha_2)\gamma_{WL}) + A\Delta\gamma \qquad (3)$$

For our discussion it is important to note that $\Delta\gamma = \gamma_{SW} + \gamma_{WL} - \gamma_{SL}$ is positive in the case of GaAs NWs on GaP and dominated by the contribution of strain energy due to the lattice mismatch.

Finally, a nucleus at position (2') is similar to (2), but with a fraction of $\vartheta_{2'}$ of the lateral area P in contact with material W:

$$\Delta I_{2'} = P(\alpha_{2'}(\gamma_{WV} - \gamma_{LV}) + (1 - \alpha_{2'} - 2\vartheta_{2'})\gamma_{WL}) + A\Delta\gamma \qquad (4)$$

We now express all extensive properties as function of the nucleus radius r: the interface area $A = \frac{c}{2}r^2$, the peripheral areas $P = \tilde{h}\, b\, r$ and the particle number $N = \rho\, A\, h = \rho\, h\, \frac{c}{2}r^2$, where h is the height of the nucleus formed by a bilayer, ρ is the number density, b and c are geometry factors. Growth starts after a nucleus surpasses a critical size of radius r_i^* where it becomes stable. This r_i^* can be found at the maximum $\frac{\partial \Delta G_i(r=r_i^*)}{\partial r} = 0$, where the formation enthalpy is $\Delta G_i^* = \Delta G_i(r_i^*)$. Specifically, this yields with $\Delta I_i = P\Gamma_i + A\Delta\gamma_i$ with $\Delta\gamma_i = 0$ in case of (1) and (1'):

$$r_i^* = \frac{\tilde{h}\, b\, \Gamma_i}{c\,(\varrho\, h\, \Delta\mu - \Delta\gamma_i)} \qquad (5)$$

$$\Delta G_i^* = \frac{\tilde{h}^2\, b^2\, \Gamma_i^2}{2c\,(\varrho\, h\, \Delta\mu - \Delta\gamma_i)} \qquad (6)$$

The probability for the formation of a nucleus at position i in a Gibbs ensemble is:

$$p_i = \frac{g_i\, \exp\left[-\frac{\Delta G_i^*}{k_B T}\right]}{\sum_j g_j \exp\left[-\frac{\Delta G_j^*}{k_B T}\right]} \qquad (7)$$

We need to include factors g_i that indicate the (relative) number of possible realizations for each position. For example, a (2') nucleus can only be realized in two possible positions at the corner ($g_{2'} = 2$), whereas many more realizations are possible for nuclei of type (2), namely along the whole lower circumference of the liquid as indicated by the dashed line in Figure 5c. As a reasonable approximation for g_2 , we take the number of atom sites (circumference divided by lattice constant). For typical sizes seen in experiment this means $g_1 = 660$, $g_{1'} = g_{2'} = 2$ and $g_2 = 1150$.

We now plug in concrete numbers for both the geometrical factors as well as the interface energies. As illustrated in Figure 5d, we consider hexagons with $\alpha_1 = \alpha_{1'} = \beta_{1'} = \alpha_2 = \alpha_{2'} = \vartheta_{2'} = \frac{1}{6}$. For a hexagon, we have $b = 6$ and $c = 3\sqrt{3}$. Values for the interface energies were taken from the literature[25,52–56] and our own DFT calculations – details are given in the Supporting Information in section S7. Note that for GaAs on GaP, $\Delta\gamma = 0.77\ \frac{eV}{nm^2}$ is dominated by the strain energy, since $\gamma_{SL} \approx \gamma_{WL}$ and the chemical contribution to γ_{SW} is vanishingly small. Furthermore, in section S8 we show that

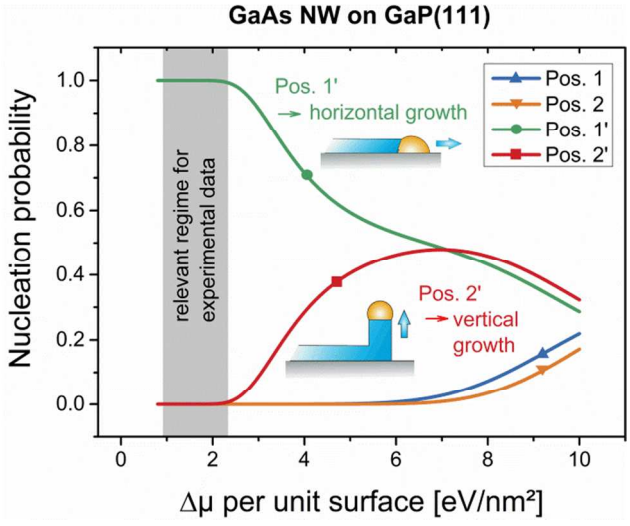

Figure 6. The probability for different nuclei in dependence of the chemical potential difference $\Delta\mu$ calculated for a horizontal GaAs NW on GaP assuming hexagonally shaped nuclei. The range of $\Delta\mu$ relevant for the experiments is highlighted in blue.

the overall trends for p_i remain unaffected even for large parameter variations and the particular nucleus shape.

GaAs nanowires. With these numerical values, we can now evaluate equation (7). The result is shown in Figure 6, where we have highlighted the relevant range of $\Delta\mu$, which corresponds to typical experimental conditions during growth.[57,58] Figure 6 involves $\Delta\mu$ per unit surface, i.e. $\Delta\mu$ multiplied by ϱh, which has the same dimension as $\Delta\gamma$. It can clearly be seen that within the experimentally relevant range, the probability for nucleation at positions (1) and (2) is vanishingly small and that position (1') is the most frequent one, *i.e.* $p_{1'} \gg p_{2'}$. There are two reasons for the preference of (1'). First, due to the contribution of $\Delta\gamma > 0$ to ΔG_i^*, nucleation at positions (2) and (2') requires a high amount of energy. Second, the primed positions (1') and (2') have a higher amount of the lateral area already in contact with substrate S or the wire W, which is again energetically preferred since the preexisting interface S-L or W-L is eliminated, respectively. Because of that, we expect only few nucleation events to take place at position (2') and most at (1'). These nuclei at (1') are likely to trigger growth of an additional GaAs layer on the inclined W-L interface, thereby continuing horizontal growth. This argument also holds if the NW grows on top of an RTB, because this defect is merely in the substrate below and does not prevent the growth of an additional layer at the W-L interface. This is illustrated in Figure 7a.

As intermediate conclusion, we note that heteroepitaxially grown NWs continue with horizontal growth once they grow horizontally for the following reason. In contrast to a homointerface, the heterointerface between nucleus and substrate results in a positive value of γ_{SW}, and hence in an increased $\Delta\gamma$ ($\Delta\gamma = \gamma_{SW} + \gamma_{WL} - \gamma_{SL}$). Since the higher the value of $\Delta\gamma$, the smaller the nucleation probability at (2'), nucleation at (1') is favored for heteroepitaxial growth of NW, so that horizontal growth is elongated. In case of GaAs NWs on GaP, γ_{SW} is dominated by strain energy, which also applies to GaAs/InAs and GaP/InP (*cf.* section S9 in the Supporting Information). Note that this finding is partially dif-

ferent from the interpretation of the growth mechanism of horizontal InAs NWs on GaAs(111)B by Zhang *et al.*,[33] who state that "the lattice mismatch only plays a minor or no role in trace formation". They argue that the different interface energies for InAs/L and GaAs/L lead to a Au-particle, which retains contact with the underlying substrate and thereby causes horizontal growth. This argument certainly is important and must be considered in the model (and is included here in $\Delta\gamma$ as $\gamma_{WL} - \gamma_{SL}$). However, their argumentation is only of thermodynamic nature and neglects both the kinetics of the growth process and the interfacial energy between substrate and NW. The influence of strain due to lattice mismatch becomes particularly important when the difference between γ_{WL} and γ_{SL} is smaller than for the material combinations studied by Zhang *et al.*

As a test of our model, we investigated the stacking fault (SF) density of horizontal and vertical GaAs NWs on GaP(111)B by TEM (see section S6 in the Supporting Information). The data give evidence that horizontal NWs are free of SFs which are parallel to its final growth front. In contrast, both the vertical NW and the initial part of the horizontal NW contain SFs that are parallel to the substrate surface. SFs are introduced when nuclei occur in SF configuration and thereby create a mirror plane with the underlying NW material. As the additional energy needed is very small (0.11 eV/nm²),[59] this defect type almost always accompanies (vertical) NW growth (*e.g.* Refs. 7,8,15, Figure S9 and inset of Figure S2c). In contrast to vertical NW growth (nucleation at (2) at a TPB), our model predicts horizontal NW growth to be triggered by nucleation at a QPB and not at a TPB, *i.e.* at (1') and not (1). Nucleation in SF configuration at position (1'), however, introduces not only a mirror plane towards the NW, but also a Σ3 {511}/{111} boundary with the substrate (comparable to RTBs). Hence, nucleation in SF configuration is significantly less likely at position (1') than at position (1) and (2). Consequentially, the absence of SFs or other defects parallel to the growth front of horizontal NWs, affirms our model and its prediction of favored nucleation at QPBs. Note that nucleation at position (1) for a horizontal NW and (2) for a vertical NW are equally likely, as both nuclei types are homoepitaxial (*cf.* next section).

GaP nanowires. For the calculation of nucleation probabilities in case of (homoepitaxial) GaP NWs, simplifications are possible: Since material W is the same as substrate S, we have $\gamma_{SW} = \gamma_{WW} = 0$ and $\gamma_{WL} = \gamma_{SL}$. Thus, $\Delta I_{1'} = \Delta I_{2'}$ and the positions (1') and (2') become equivalent, *i.e.* $p_{1'} = p_{2'}$ (≈ 0.5 for $\Delta\mu\rho h < 7\ eV/nm^2$ as shown in Figure 8 for $x = 1$). Therefore, nuclei will form both at (1') and (2'). Just as in the heteroepitaxial case, nucleation events at position (1') are associated with continued horizontal NW growth. The higher probability at (2') in the homoepitaxial case requires a more detailed discussion of the effects of nucleation at this position: If the gold droplet is not on top of an RTB, the nucleus can grow unhindered to cover the entire S-L interface. This in turn is likely to separate the liquid gold from the GaP below, thereby starting vertical NW growth. This will eventually happen once a sufficient number of successive nucleation events with subsequent layer growth have occurred. If, on the other hand, growth happens on top of an RTB, we argue that elongated lateral growth is the likely outcome. The corresponding situation is sketched in Figure 7b. The boundary between the two domains (termed α and

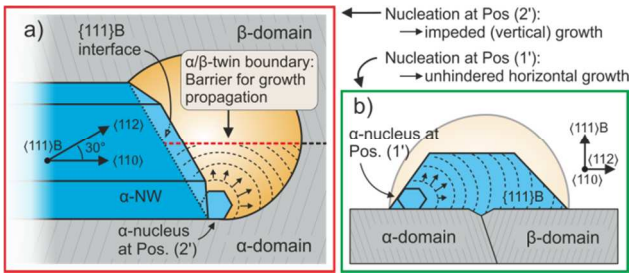

Figure 7. Schematic illustrations of a horizontal NW on a rotational twin boundary (RTB). The top view in (a) illustrates how a nucleus at position (2') extends and forms only half a layer due to the twin boundary. The front view in (b) along the ⟨110⟩ growth direction shows nucleation at position (1'). Here, a complete NW layer can be formed resulting in horizontal growth. Note that the growth front is {111}B is pointing in a ⟨112⟩ direction, but growth occurs in ⟨110⟩ direction due to the Au- trapping caused by the RTB.

β) provides a barrier to growth, because of the local stress at this boundary and since the atomic configurations of the α- and β-domains do not allow direct continuation of a GaP bilayer on top of the RTB. Therefore, nucleation at (2') on top of an α-domain near an RTB likely results in only partial coverage of the S-L interface. Hence, a complete separation of the gold droplet from the substrate would only be possible if another nucleus on the corresponding β-domain formed simultaneously, which is rather unlikely (*inter alia* due to stacking fault configuration of an α nucleus on the β-domain). Consequentially, the model also explains why (homoepitaxial) GaP NWs grow horizontally along RTBs and continue with vertical growth, once they leave the RTB. A similar argumentation can explain the frequent observation of Au-particles without NW growth, which is described in section S4 of the Supporting Information.

GaAsP nanowires and other hetero-systems. Additionally, we studied experimentally the growth of $GaAs_{x-1}P_x$ NWs on GaP(111)B and calculated nucleation probabilities for this and other hetero-systems (see Figure 8 and section S9 in the Supporting Information). Figure 8a predicts nucleation probabilities for GaAsP NWs of different composition. Naturally, the probability of nucleation at position (2') increases with higher P-ratios due to the decreasing lattice mismatch. Accordingly, a sufficiently high number of successive nucleation events at (2'), triggering vertical growth, becomes more likely with increasing P-ratio. This prediction is indeed confirmed by experiment. Panel b and c of Figure 8 compare $GaAs_{x-1}P_x$ NWs with two different group-V-precursor ratios and hence two different compositions. In both cases nucleation conditions led exclusively to growth of NWs, which are initially horizontal. While for the lower P ratio none of the NWs changes its growth direction from horizontal to vertical (in analogy to pure GaAs NWs), around 5 % of the NWs do so for the higher P ratio. Importantly, this growth direction change is not triggered by impingement on other horizontal NWs, as sometimes reported in literature.[33,35,60] To our knowledge, this is the first report of a change in growth direction from horizontal to out-of-plane for a hetero-system (where the NW does not encounter another NW or object). The calculated nucleation probabilities of the other (binary) III-V hetero-systems (InP NWs on GaP or GaAs, InAs NWs

on GaAs) show a dependence on the chemical potential very similar to GaAs NWs on GaP (compare Figure 6 with Figure S14). Here as well, nucleation at position (1') is favored over a wide range of $\Delta\mu$, since nucleation at (2') involves a lot of strain energy – and in case of InAs NWs on GaP, also a significant amount of chemical energy (*cf.* Table S1 in the Supporting Information).

As mentioned in the introduction, there exists a variety of lattice-mismatched systems, including elementary, III-V, oxide- and selenide materials, where horizontal NW growth is reported.[33–41,61–65] We are convinced that the principal idea of our model can explain the elongated growth of horizontal NWs in all these studies – despite substantial differences to our systems. These differences may correspond to different crystal structures and orientations,[34,62] magnitude in lattice-mismatch, type of catalyst *et cetera*. The key argument remains the same: nucleation and subsequent layer growth will by far be more likely at the NW/catalyst interface (at position (1')) than at the substrate/catalyst interface (position (2')), since the latter is impeded by strain and chemical dissimilarity. This claim is supported by the fact that in none of these studies, NW material is visible directly between the catalyst and the substrate surface.

Conclusion

We have found a strong detrimental effect of rotational twin boundaries (RTBs) on VLS growth of NWs: RTBs tend to trap Au droplets, which causes either completely suppressed or non-vertical growth of NWs. When nucleated at RTBs, the lattice-mismatch between NW and substrate is decisive for the final growth direction: While homoepitaxial NWs may grow diagonally or horizontally, heteroepitaxial NWs grow persistently horizontally, also away from the RTBs. Homoepitaxial NWs, in contrast, switch to vertical growth away from the RTBs. The suppression of rotational twins in the transition-layer is therefore particularly relevant in the case of heteroepitaxial NW growth.

We developed a quantitative model based on classical nucleation theory, which shows that the lattice mismatch between substrate and NW plays an essential role for the nucleus location and thereby the growth direction. Nuclei triggering vertical growth have to form on top of the substrate surface, which involves significant strain energy. Therefore, (strain-free) nuclei at the catalyst-NW interface are favored, leading to horizontal growth. Here, nucleation at the quadruple phase boundary is strongly favored over nucleation at the triple phase boundary (no contact with the substrate), which explains the prevalent observation of defect-free horizontal NW growth. Extending our model could also deepen the understanding of homoepitaxial NW growth on differently oriented substrates as well as vertical versus horizontal NW growth in non-III-V-systems.

METHODS

Both NW and GaP layer growth were carried out by metalorganic vapor phase epitaxy (MOVPE) in an Aixtron AIX 200 reactor with H_2 as carrier gas at 50 mbar with a total flow of 7.1 L/min during layer growth and 3.4 L/min during NW preparation.

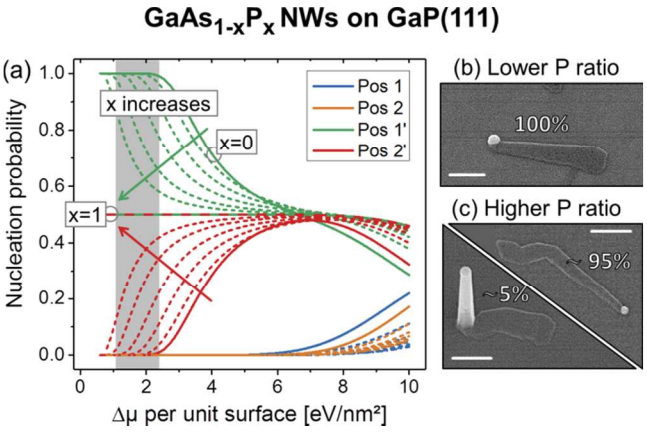

Figure 8. (a) Nucleation probabilities for horizontal $GaAs_{1-x}P_x$ NWs grown on GaP(111)B with x ranging from 0 to 1 ($x \in \{0, 0.05, 0.1, 0.2, 0.35, 0.6, 1\}$), *i.e.* pure GaAs and GaP, respectively. Geometrical parameters are chosen in analogy to Figure 6 and interfacial energies are interpolated linearly between both extremes (*cf.* section S9). (b) and (c) show horizontal GaAsP NWs on GaP(111)B with two different compositions. While for the lower P ratio all NWs remain horizontal, around 5% of the NWs become vertical for the higher P ratio. The scale bars are 200 nm. For SEM overview scans the reader is referred to Figure S13 in the Supporting Information.

For the preparation of the GaP/Si hetero-substrates, Si(111) substrates with 3° miscut in [11-2] direction were used. Prior to growth, the substrates were wet-chemically treated by the RCA clean procedure with buffered oxide etch (BOE), and thermally deoxidized in the MOVPE reactor.[66] The Si(111) surface was then exposed to tertiarybutylarsine (TBAs) to allow for growth of GaP with B-type polarity.[23] A two-step process for the growth of GaP layers was applied with a nucleation phase at low temperatures (either 420°C or 500°C) for 15 min and subsequent growth at 660°C for further 45 min, resulting in GaP layers with a thickness of around 100 nm. While the nucleation at 420°C leads to a low density of twins (below 8%), nucleation at 500°C results in a significantly higher one (~30%). For further details see Ref. 22.
NWs were grown by the Au-mediated VLS mode on these GaP/Si hetero-substrates with different twin density and on GaP(111)B 3° wafer pieces as a reference free of rotational twins. Prior to NW growth, the substrates were cleaned in acetone and isopropyl alcohol, and subsequently Au particles of ca. 100 nm diameter were deposited from colloidal solution. To desorb oxides from the surface, the samples were loaded into the reactor and annealed for 10 minutes at 600°C with continuous phosphorus stabilization using tertiarybutylphosphine (TBP) as precursor to prevent substrate decomposition. Subsequently, GaP (GaAs) NW growth was performed by supplying trimethylgallium (TMGa) for 10 min (1 min) with a molar fraction of $\chi_{TMGa} = 6.16 \times 10^{-5}$ (1.26×10^{-4}) at 500°C (450°C) with a TBP/TMGa (TBAs/TMGa) ratio of 10 (2.5). The growth duration of the GaAs NWs was intentionally kept short to facilitate their characterization. The GaAsP NWs were grown at 475°C for 12 minutes with a V/III of 20 and a TBP/V of 0.5 for the lower and 0.75 for the higher P-ratio, respectively. All temperatures mentioned were measured by a thermocouple within the graphite suszeptor.

All samples were characterized by means of high resolution scanning electron microscopy (SEM, Hitachi S 4800-II). The majority of NWs were measured under different angels to determine their spatial growth direction. Transmission electron microscopy (TEM, Jeol ARM200F) was applied to investigate the crystal structure of selected GaAs NWs grown on GaP(111)B. In order to determine the (volumetric) twin density of GaP layers on Si, high resolution x-ray diffraction measurements (HR XRD, Bruker AXS D8 Discover) were performed.[22]

ASSOCIATED CONTENT

Supporting Information

Supporting Information available: Nanowire growth on reference samples (Section S1), elevation and azimuth angle for diagonal GaP nanowires (Section S2), different horizontal GaAs nanowires on GaP/Si (Section S3), SEM data and discussion of Au-particles without nanowire 'Au only' (Section S4), growth facets of horizontal GaAs nanowires on GaP(111)B (Section S5), TEM investigation of GaAs nanowires on GaP(111)B (Section S6), numerical values for model parameters (Section S7), sensitivity on model parameters (Section S8), GaAsP nanowires and other hetero-systems (Section S9). The Supporting Information is available free of charge on the ACS Publications website as PDF.

AUTHOR INFORMATION

Corresponding Author

*E-mail: matthias.steidl@tu-ilmenau.de. Tel.: +49 3677 69-2578. *E-mail: thomas.hannappel@tu-ilmenau.de. Tel.: +49 3677 69- 2566.

Author Contributions

‡These authors contributed equally.

Notes

The authors declare no competing financial interests.

ACKNOWLEDGMENT

This work was financially supported by the BMBF (Project No. 03SF0404A) and partly by the Spanish Ministry of Economy (project TEC2014-54260-C3-2-P). C.K. and L.W. acknowledge the Thuringia Graduate School for Photovoltaics "Photograd" for financial support. The authors would like to thank A. Paszuk and A. Nägelein for valuable discussions as well as A. Müller and M. Biester for technical support, T. Nieszner for supporting the determination of the spatial direction of NWs and D. Roßberg for preparing the TEM lamella.

REFERENCES

(1) Bakkers, E.; Borgstrom, M.; Verheijen, M. Epitaxial Growth of III-V Nanowires on Group IV Substrates. *MRS Proc.* **2008**, *1068*, 1068-C02-4.

(2) Mårtensson, T.; Svensson, C. P. T.; Wacaser, B. a; Larsson, M. W.; Seifert, W.; Deppert, K.; Gustafsson, A.; Wallenberg, L. R.; Samuelson, L. Epitaxial III – V Nanowires on Silicon. *Nano Lett.* **2004**, *4*, 1987–1990.

(3) Bao, X.-Y.; Soci, C.; Susac, D.; Bratvold, J.; Aplin, D. P. R.; Wei, W.; Chen, C.-Y.; Dayeh, S. a; Kavanagh, K. L.; Wang, D. Heteroepitaxial Growth of Vertical GaAs Nanowires on Si(111) Substrates by Metal-Organic Chemical Vapor Deposition. *Nano Lett.* **2008**, *8*, 3755–3760.

(4) Fonseka, H. A.; Tan, H. H.; Wong-Leung, J.; Kang, J. H.; Parkinson, P.; Jagadish, C. High Vertical Yield InP Nanowire Growth on Si(111) Using a Thin Buffer Layer. *Nanotechnology* **2013**, *24*, 465602.

(5) Wagner, R. S.; Ellis, W. C. Vapor-Liquid-Solid Mechanism of Single Crystal Growth. *Appl. Phys. Lett.* **1964**, *4*, 89.

(6) Dick, K. A. A Review of Nanowire Growth Promoted by Alloys and Non-Alloying Elements with Emphasis on Au-Assisted III–V Nanowires. *Prog. Cryst. Growth Charact. Mater.* **2008**, *54*, 138–173.

(7) Joyce, H. J.; Gao, Q.; Hoe Tan, H.; Jagadish, C.; Kim, Y.; Zou, J.; Smith, L. M.; Jackson, H. E.; Yarrison-Rice, J. M.; Parkinson, P.; *et al.* III–V Semiconductor Nanowires for Optoelectronic Device Applications. *Prog. Quantum Electron.* **2011**, *35*, 23–75.

(8) Zhang, Y.; Wu, J.; Aagesen, M.; Liu, H. III–V Nanowires and Nanowire Optoelectronic Devices. *J. Phys. D. Appl. Phys.* **2015**, *48*, 463001.

(9) Piscopiello, E.; Tapfer, L.; Antisari, M. V.; Paiano, P.; Prete, P.; Lovergine, N. Formation of Epitaxial Gold Nanoislands on (100) Silicon. *Phys. Rev. B - Condens. Matter Mater. Phys.* **2008**, *78*, 1–7.

(10) Roest, A. L.; Verheijen, M. A.; Wunnicke, O.; Serafin, S.; Wondergem, H.; Bakkers, E. P. A. M. Position-Controlled Epitaxial III–V Nanowires on Silicon. *Nanotechnology* **2006**, *17*, S271–S275.

(11) Evans, M. J.; Stavola, M.; Weinstein, M. G.; Uftring, S. J. Vibrational Spectroscopy of Defect Complexes Containing Au and H in Si. *Mater. Sci. Eng. B* **1999**, *58*, 118–125.

(12) Steger, M.; Yang, A.; Sekiguchi, T.; Saeedi, K.; Thewalt, M. L. W.; Henry, M. O.; Johnston, K.; Riemann, H.; Abrosimov, N. V.; Churbanov, M. F.; *et al.* Photoluminescence of Deep Defects Involving Transition Metals in Si: New Insights from Highly Enriched 28Si. *J. Appl. Phys.* **2011**, *110*, 81301.

(13) Dick, K. A.; Deppert, K.; Samuelson, L.; Wallenberg, L. R.; Ross, F. M. Control of GaP and GaAs Nanowire Morphology through Particle and Substrate Chemical Modification. *Nano Lett.* **2008**, *8*, 4087–4091.

(14) Huang, H.; Ren, X.; Ye, X.; Guo, J.; Wang, Q.; Yang, Y.; Cai, S.; Huang, Y. Growth of Stacking-Faults-Free Zinc Blende GaAs Nanowires on Si Substrate by Using AlGaAs/GaAs Buffer Layers. *Nano Lett.* **2010**, *10*, 64–68.

(15) Kang, J. H.; Gao, Q.; Joyce, H. J.; Tan, H. H.; Jagadish, C.; Kim, Y.; Choi, D. Y.; Guo, Y.; Xu, H.; Zou, J.; *et al.* Novel Growth and Properties of GaAs Nanowires on Si Substrates. *Nanotechnology* **2010**, *21*, 35604.

(16) Miccoli, I.; Prete, P.; Marzo, F.; Cannoletta, D.; Lovergine, N. Synthesis of Vertically-Aligned GaAs Nanowires on GaAs/(111)Si Hetero-Substrates by Metalorganic Vapour Phase Epitaxy. In *Crystal Research and Technology*; 2011; Vol. 46, pp. 795–800.

(17) Ghalamestani, S. G.; Johansson, S.; Borg, B. M.; Dick, K. A.; Wernersson, L.-E. Highly Controlled InAs Nanowires on Si(111) Wafers by MOVPE. *Phys. Status Solidi* **2012**, *9*, 206–209.

(18) Salomon, D.; Dussaigne, A.; Lafossas, M.; Durand, C.; Bougerol, C.; Ferret, P.; Eymery, J. Metal Organic Vapour-Phase Epitaxy Growth of GaN Wires on Si (111) for Light-Emitting Diode Applications. *Nanoscale Res. Lett.* **2013**, *8*, 61.

(19) Songmuang, R.; Landré, O.; Daudin, B. From Nucleation to Growth of Catalyst-Free GaN Nanowires on Thin AlN Buffer Layer. *Appl. Phys. Lett.* **2007**, *91*, 251902.

(20) Proessdorf, A.; Grosse, F.; Romanyuk, O.; Braun, W.; Jenichen, B.; Trampert, A.; Riechert, H. Interface Engineering for Improved Growth of GaSb on Si(111). *J. Cryst. Growth* **2011**, *323*, 401–404.

(21) Suzuki, H.; Ito, D.; Fukuyama, A.; Ikari, T. Reduction of Rotational Twin Formation by Indium Pre-Evaporation in

Epitaxially Grown GaAs Films on Si (111) Substrate. *J. Cryst. Growth* **2013**, *380*, 148–152.

(22) Koppka, C.; Paszuk, A.; Steidl, M.; Supplie, O.; Kleinschmidt, P.; Hannappel, T. Suppression of Rotational Twin Formation in Virtual GaP/Si(111) Substrates for III–V Nanowire Growth. *Cryst. Growth Des.* **2016**, *16*, 6208–6213.

(23) Paszuk, A.; Brückner, S.; Steidl, M.; Zhao, W.; Dobrich, A.; Supplie, O.; Kleinschmidt, P.; Prost, W.; Hannappel, T. Controlling the Polarity of Metalorganic Vapor Phase Epitaxy-Grown GaP on Si (111) for Subsequent III-V Nanowire Growth. *Appl. Phys. Lett.* **2015**, *106*, 231601.

(24) Wacaser, B. a.; Dick, K. a.; Johansson, J.; Borgström, M. T.; Deppert, K.; Samuelson, L. Preferential Interface Nucleation: An Expansion of the VLS Growth Mechanism for Nanowires. *Adv. Mater.* **2009**, *21*, 153–165.

(25) Glas, F.; Harmand, J.-C.; Patriarche, G. Why Does Wurtzite Form in Nanowires of III-V Zinc Blende Semiconductors? *Phys. Rev. Lett.* **2007**, *99*, 146101.

(26) Dubrovskii, V. G. Theory of VLS Growth of Compound Semiconductors. In *Semiconductors and Semimetals*; 2015; pp. 1–78.

(27) Joyce, H. J.; Wong-Leung, J.; Gao, Q.; Tan, H. H.; Jagadish, C. Phase Perfection in Zinc Blende and Wurtzite III–V Nanowires Using Basic Growth Parameters. *Nano Lett.* **2010**, *10*, 908–915.

(28) Assali, S.; Gagliano, L.; Oliveira, D. S.; Verheijen, M. a.; Plissard, S. R.; Feiner, L. F.; Bakkers, E. P. a M. Exploring Crystal Phase Switching in GaP Nanowires. *Nano Lett.* **2015**, *15*, 8062–8069.

(29) Dubrovskii, V. G.; Grecenkov, J. Zeldovich Nucleation Rate, Self-Consistency Renormalization, and Crystal Phase of Au-Catalyzed Gaas Nanowires. *Cryst. Growth Des.* **2015**, *15*, 340–347.

(30) Algra, R. E.; Verheijen, M. a.; Feiner, L. F.; Immink, G. G. W.; Theissmann, R.; Van Enckevort, W. J. P.; Vlieg, E.; Bakkers, E. P. a M. Paired Twins and {11-2} Morphology in GaP Nanowires. *Nano Lett.* **2010**, *10*, 2349–2356.

(31) Breuer, S.; Feiner, L. F.; Geelhaar, L. Droplet Bulge Effect on the Formation of Nanowire Side Facets. *Cryst. Growth Des.* **2013**, *13*, 2749–2755.

(32) Jiang, N.; Wong-Leung, J.; Joyce, H. J.; Gao, Q.; Tan, H. H.; Jagadish, C. Understanding the True Shape of Au-Catalyzed GaAs Nanowires. *Nano Lett.* **2014**, *14*, 5865–5872.

(33) Zhang, X.; Zou, J.; Paladugu, M.; Guo, Y.; Wang, Y.; Kim, Y.; Joyce, H. J.; Gao, Q.; Tan, H. H.; Jagadish, C. Evolution of Epitaxial InAs Nanowires on GaAs (111)B. *Small* **2009**, *5*, 366–369.

(34) Du, W.; Yang, X.; Pan, H.; Ji, X.; Ji, H.; Luo, S.; Zhang, X.; Wang, Z.; Yang, T. Controlled-Direction Growth of Planar InAsSb Nanowires on Si Substrates without Foreign Catalysts. *Nano Lett.* **2016**, *16*, 877–882.

(35) Breuer, S.; Hilse, M.; Trampert, a.; Geelhaar, L.; Riechert, H. Vapor-Liquid-Solid Nucleation of GaAs on Si(111): Growth Evolution from Traces to Nanowires. *Phys. Rev. B - Condens. Matter Mater. Phys.* **2010**, *82*, 1–7.

(36) Zhang, C.; Miao, X.; Mohseni, P. K.; Choi, W.; Li, X. Site-Controlled VLS Growth of Planar Nanowires: Yield and Mechanism. *Nano Lett.* **2014**, *14*, 6836–6841.

(37) Zi, Y.; Jung, K.; Zakharov, D.; Yang, C. Understanding Self-Aligned Planar Growth of InAs Nanowires. *Nano Lett.* **2013**, *13*, 2786–2791.

(38) Wallentin, J.; Kriegner, D.; Stangl, J.; Borgström, M. T. Au-Seeded Growth of Vertical and in-Plane III-V Nanowires on Graphite Substrates. *Nano Lett.* **2014**, *14*, 1707–1713.

(39) Munshi, A. M.; Dheeraj, D. L.; Fauske, V. T.; Kim, D. C.; Van Helvoort, A. T. J.; Fimland, B. O.; Weman, H. Vertically Aligned GaAs Nanowires on Graphite and Few-Layer Graphene: Generic Model and Epitaxial Growth. *Nano Lett.* **2012**, *12*, 4570–4576.

(40) Nikoobakht, B.; Michaels, C. A.; Stranick, S. J.; Vaudin, M. D. Horizontal Growth and in Situ Assembly of Oriented Zinc Oxide Nanowires. *Appl. Phys. Lett.* **2004**, *85*, 3244.

(41) Levin, I.; Davydov, A.; Nikoobakht, B.; Sanford, N.; Mogilevsky, P. Growth Habits and Defects in ZnO Nanowires Grown on GaN/sapphire Substrates. *Appl. Phys. Lett.* **2005**, *87*, 24–27.

(42) Shalev, E.; Oksenberg, E.; Rechav, K.; Popovitz-Biro, R.; Joselevich, E. Guided CdSe Nanowires Parallelly Integrated into Fast Visible-Range Photodetectors. *ACS Nano* **2017**, *11*, 213–220.

(43) Oksenberg, E.; Popovitz-Biro, R.; Rechav, K.; Joselevich, E. Guided Growth of Horizontal ZnSe Nanowires and Their Integration into High-Performance Blue-UV Photodetectors. *Adv. Mater.* **2015**, *27*, 3999–4005.

(44) Narayanan, V.; Mahajan, S.; Bachmann, K. J.; Woods, V.; Dietz, N. Stacking Faults and Twins in Gallium Phosphide Layers Grown on Silicon. *Philos. Mag. A* **2002**, *82*, 685–698.

(45) Karlsson, L. S.; Johansson, J.; Svensson, C. P. T.; Mårtensson, T.; Wacaser, B. A.; Malm, J.-O.; Deppert, K.; Seifert, W.; Samuelson, L.; Wallenberg, L. R. Structural Characterisation of GaP <111>B Nanowires by HRTEM. In *Microscopy of Semiconducting Materials 2007*; Cullis, A. G.; Midgley, P. A., Eds.; Springer Netherlands: Dordrecht, 2008; pp. 229–232.

(46) Fortuna, S. A.; Li, X. Metal-Catalyzed Semiconductor Nanowires: A Review on the Control of Growth Directions. *Semicond. Sci. Technol.* **2010**, *25*, 24005.

(47) Algra, R. E.; Verheijen, M. a; Borgström, M. T.; Feiner, L.-F.; Immink, G.; van Enckevort, W. J. P.; Vlieg, E.; Bakkers, E. P. a M. Twinning Superlattices in Indium Phosphide Nanowires. *Nature* **2008**, *456*, 369–372.

(48) Akiyama, T.; Haneda, Y.; Nakamura, K.; Ito, T. Role of the Au/GaAs(111) Interface on the Wurtzite-Structure Formation during GaAs Nanowire Growth by a Vapor-Liquid-Solid Mechanism. *Phys. Rev. B - Condens. Matter Mater. Phys.* **2009**, *79*, 1–4.

(49) Uccelli, E.; Arbiol, J.; Magen, C.; Krogstrup, P.; Russo-Averchi, E.; Heiss, M.; Mugny, G.; Morier-Genoud, F.; Nygård, J.; Morante, J. R.; *et al.* Three-Dimensional Multiple-Order Twinning of Self-Catalyzed GaAs Nanowires on Si Substrates. *Nano Lett.* **2011**, *11*, 3827–3832.

(50) Bauer, J.; Pietsch, U.; Davydok, A.; Biermanns, A.; Grenzer, J.; Gottschalch, V.; Wagner, G. X-Ray Investigation of the Interface Structure of Free Standing InAs Nanowires Grown on GaAs [(1)over-bar(1)over-bar(1)over-bar](B). *Appl. Phys. a-Materials Sci. Process.* **2009**, *96*, 851–859.

(51) Ross, F. M. Controlling Nanowire Structures through Real Time Growth Studies. *Rep. Prog. Phys. Rep. Prog. Phys* **2010**, *73*, 114501–114521.

(52) Glas, F. Critical Dimensions for the Plastic Relaxation of Strained Axial Heterostructures in Free-Standing Nanowires. *Phys. Rev. B* **2006**, *74*, 121302.

(53) Glas, F.; Ramdani, M. R.; Patriarche, G.; Harmand, J.-C. Predictive Modeling of Self-Catalyzed III-V Nanowire Growth. *Phys. Rev. B* **2013**, *88*, 195304.

(54) Jasper, J. J. The Surface Tension of Pure Liquid Compounds. *J. Phys. Chem. Ref. Data* **1972**, *1*, 841.

(55) Moll, N.; Kley, A.; Pehlke, E.; Scheffler, M. GaAs Equilibrium Crystal Shape from First Principles. *Phys. Rev. B* **1996**, *54*, 8844–8855.

(56) Zangwill, A. *Physics at Surfaces*; Cambridge University Press: Cambridge, 1988.

(57) Algra, R. E.; Verheijen, M. a; Feiner, L.-F.; Immink, G. G. W.; Enckevort, W. J. P. Van; Vlieg, E.; Bakkers, E. P. a M. The Role of Surface Energies and Chemical Potential during Nanowire Growth. *Nano Lett.* **2011**, *11*, 1259–1264.

(58) Glas, F. Chemical Potentials for Au-Assisted Vapor-Liquid-Solid Growth of III-V Nanowires. *J. Appl. Phys.* **2010**, *108*.

(59) Glas, F. A Simple Calculation of Energy Changes upon Stacking Fault Formation or Local Crystalline Phase Transition in Semiconductors. *J. Appl. Phys.* **2008**, *104*.

(60) Dick, K. A.; Kodambaka, S.; Reuter, M. C.; Deppert, K.;

Samuelson, L.; Seifert, W.; Wallenberg, L. R.; Ross, F. M. The Morphology of Axial and Branched Nanowire Heterostructures. *Nano Lett.* **2007**, *7*, 1817–1822.

(61) Mataev, E.; Rastogi, S. K.; Madhusudan, A.; Bone, J.; Lamprinakos, N.; Picard, Y.; Cohen-Karni, T. Synthesis of Group IV Nanowires on Graphene: The Case of Ge Nanocrawlers. *Nano Lett.* **2016**, *16*, 5267–5272.

(62) Shen, Y.; Turner, S.; Yang, P.; Van Tendeloo, G.; Lebedev, O. I.; Wu, T. Epitaxy-Enabled Vapor-Liquid-Solid Growth of Tin-Doped Indium Oxide Nanowires with Controlled Orientations. *Nano Lett.* **2014**, *14*, 4342–4351.

(63) Tsivion, D.; Schvartzman, M.; Popovitz-Biro, R.; von Huth, P.; Joselevich, E. Guided Growth of Millimeter-Long Horizontal Nanowires with Controlled Orientations. *Science (80-.).* **2011**, *333*, 1003–1007.

(64) Tsivion, D.; Joselevich, E. Guided Growth of Epitaxially Coherent GaN Nanowires on SiC. *Nano Lett.* **2013**, *13*, 5491–5496.

(65) Kim, W.; Kim, D.; Hong, S. Lateral Epitaxial Growth of Faceted SnO_2 Nanowires with Self-Alignment. *CrystEngComm* **2014**, *16*, 9340–9344.

(66) Zhao, W.; Steidl, M.; Paszuk, A.; Brückner, S.; Dobrich, A.; Supplie, O.; Kleinschmidt, P.; Hannappel, T. Analysis of the Si(111) Surface Prepared in Chemical Vapor Ambient for Subsequent III-V Heteroepitaxy. *Appl. Surf. Sci.* **2017**, *392*, 1043–1048.

Keywords:

III-V on silicon; preferential interface nucleation; transition-layer; nucleation model; nanowire growth directions; planar nanowires; 3D twinning

Graphic for the Table of Contents